

Coherent states in magnetized anisotropic 2D-Dirac materials

E Díaz-Bautista^{*1}, M Oliva-Leyva^{†1}, Y Concha-Sánchez^{‡2}, and A Raya^{§3}

¹Physics Department, Cinvestav, P.O. Box. 14-740, 07000 Mexico City, Mexico

²Facultad de Ingeniería Civil, Universidad Michoacana de San Nicolás de Hidalgo, Edificio C, Ciudad Universitaria. Francisco J. Mújica s/n. Col. Felicitas del Río. 58030 Morelia, Michoacán, México

³Instituto de Física y Matemáticas, Universidad Michoacana de San Nicolás de Hidalgo, Edificio C-3, Ciudad Universitaria. Francisco J. Mújica s/n. Col. Felicitas del Río. 58040 Morelia, Michoacán, México

Abstract

In this work, we construct coherent states for electrons in anisotropic 2D-Dirac materials immersed in a uniform magnetic field perpendicularly oriented to the sample. In order to describe the bidimensional effects on electron dynamics in a semiclassical approach, we adopt the symmetric gauge vector potential to describe the external magnetic field through a vector potential. By solving a Dirac-like equation with an anisotropic Fermi velocity, we identify two sets of scalar ladder operators that allow us to define generalized annihilation operators, which are generators of either the Heisenberg-Weyl or $su(1,1)$ algebra. We construct both bidimensional and $su(1,1)$ coherent states as eigenstates of such annihilation operators with complex eigenvalues. In order to illustrate the effects of the anisotropy on these states, we obtain their probability density and mean energy value. Depending upon the anisotropy, expressed by the ration between the Fermi velocities along the x - and y -axes, the shape of the probability density is modified on the xy -plane with respect to the isotropic case and according to the classical dynamics.

1 Introduction

Material science has experienced a tremendous revolution after the first isolation of graphene samples [1–3], the first member of a larger class of materials nowadays dubbed generically as 2D-Dirac materials (2D-DM), which include topological insulators [4,5] and organic conductors

^{*}ediaz@fis.cinvestav.mx

[†]moliva@fis.cinvestav.mx

[‡]yconcha@umich.mx

[§]raya@ifm.umich.mx

[6, 7]. In general, these materials are characterized because at low-energy the behavior of its charge carriers is quite similar to that of ultra-relativistic fermions, given the linear nature of their dispersion relation. As a consequence, these quasi-particles are better described by a Dirac-like equation, instead of the ordinary Schrödinger equation with a typical parabolic dispersion relation. Such a description encodes the chiral and pseudo-relativistic behavior of the charge carriers that make it difficult to confine these quasi-particles through, for example, electrostatic barriers. Various proposals have been raised to address this problem, among them, to induce quasi-bounded states of massless Dirac fermions by the influence of magnetic fields. Another alternative to control the confinement and transport of charge carriers in materials that are not intrinsically anisotropic, like graphene, comes from strain engineering. In this connection, *straintronics* [8] has emerged as the field that explores how mechanical deformations of graphene flakes modify its electric properties [9]. Because, in general, the strain tensor depends on the coordinates of the membrane, one particular effect arising from mechanical deformation is that an applied strain causes electrons to behave as if they were immersed in a fictitious magnetic field, a situation that has provided interesting theoretical [9] and experimental [10] results. In contrast, uniform uniaxial strain modifies the Fermi velocity in the low-energy regime without generating any pseudo-magnetic fields [11–13] but still induces a tensor character to the Fermi velocity in the material and consequently, the dispersion relation is modified from the ideal case and the low-energy regime corrects the equations of motion still in a tractable form.

Nowadays, an increasing interest in exploring the anisotropy effects to control other physical properties of 2D-DM, e.g., its rigidity, resistance and optical conductivity [14], has arisen. In this way, the construction of coherent states in pristine graphene as carried out in Ref. [15] can be extended to anisotropic Dirac fermion systems in order to give a semi-classical description of phenomena related to the combined effects of both magnetic fields and anisotropy [16]. The latter allows to analyze a variety of properties of these materials [17–22].

Following the previous approach, the physical problem of a spinless particle moving in the xy -plane under the action of a uniform magnetic field \vec{B}_0 has been solved in the so-called symmetric gauge [23–25]

$$\vec{A} = \frac{1}{2}[\vec{B}_0 \times \vec{r}] = \frac{B_0}{2}(-y, x, 0), \quad (1)$$

and in which has made possible to build coherent states [26] as bidimensional generalizations of the Glauber states [27], starting from the results obtained by Landau [28]. Thus, one can seek to generalize this formalism in the case of anisotropic 2D-DM considering initially homogeneous perpendicular magnetic fields for describing the charge carrier dynamics as in Ref. [16], where the problem has been addressed in a Landau-like gauge with translational invariance and that conforms a first attempt for a semi-classical formulation in this kind of materials. However, if one would want to apply the coherent state formalism to investigate, for instance, some thermodynamical quantities of interest in magnetized systems, such description is limited due to the intrinsic bidimensional nature of the problem, so that it is necessary to implement the symmetric gauge [29–33].

Hence, we start from the time-independent anisotropic Dirac equation,

$$H\Psi = (v_x\sigma_x\pi_x + v_y\sigma_y\pi_y)\Psi = E\Psi, \quad (2)$$

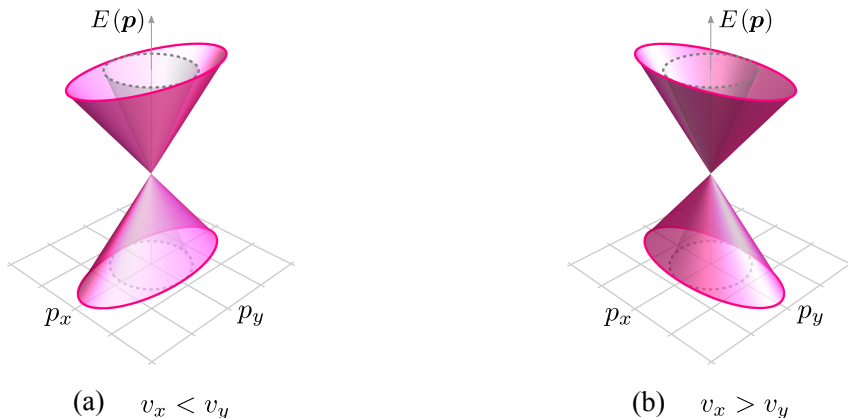


Figure 1: Dirac cones for an isotropic (dashed gray lines) and anisotropic case (solid pink contour). Dirac cone projections on the horizontal plane are ellipses whose semi-major axis is along either of the p_x -axis or of the p_y -axis.

where $v_{x/y}$ is the particle velocity in the x/y -direction and that is modified by the anisotropy –although the Fermi velocity has a tensorial character in a general sense, one can choose an appropriate coordinate system where the tensor is diagonal [14]–, $\sigma_{x/y}$ are the Pauli matrices, $\pi_{x/y} = (p_{x,y} + (e/c)A_{x/y})$ is the canonical momentum with \vec{A} given in Eq. (1) and $\Psi = (\psi_1 \ \psi_2)^T$ are the two-component wavefunctions. This framework can be considered as a generalization of Refs. [15, 34]. From here, we start the construction of coherent states, which we outline in the remaining of this article, organized as follows: In Sec. 2, the anisotropic Dirac equation is solved by employing the symmetric gauge with an anisotropy dimensionless parameter, and its associated algebraic structure is discussed. In Sec. 3, coherent states for graphene that preserve a rotational-like invariance are presented as eigenstates of matrix annihilation operators. Also, the corresponding probability and mean energy are evaluated. Our final remarks are presented in Sec. 4.

2 Anisotropic Dirac Hamiltonian

By considering the symmetric gauge vector potential (1) in Eq. (2), Dirac Hamiltonian H is rewritten as follows

$$H = \sqrt{\omega_B} \hbar v_F' \begin{bmatrix} 0 & -iA_\zeta^- \\ iA_\zeta^+ & 0 \end{bmatrix}, \quad (3)$$

after defining the ladder operators

$$A_\zeta^\pm = \mp \frac{i}{\sqrt{\omega_B} \hbar} \left[\zeta^{1/2} \left(p_x - \frac{eB_0}{2c} y \right) = \pm i \zeta^{-1/2} \left(p_y + \frac{eB_0}{2c} x \right) \right], \quad (4)$$

that satisfy the commutation relation

$$[A_\zeta^-, A_\zeta^+] = 1, \quad (5)$$

where $\omega_B = 2eB_0/c\hbar$ is the cyclotron frequency, $v'_F = \sqrt{v_x v_y}$ and $\zeta = v_x/v_y$ depends on the anisotropy direction (see Fig. 1).

The eigenvalue equation (3) gives place to two coupled equations that can be decoupled to obtain the following equations for each pseudo-spinor component,

$$\mathcal{H}^- \psi_1(x, y) = A_\zeta^- A_\zeta^+ \psi_1(x, y) = \mathcal{E} \psi_1(x, y), \quad (6a)$$

$$\mathcal{H}^+ \psi_2(x, y) = A_\zeta^+ A_\zeta^- \psi_2(x, y) = \mathcal{E} \psi_2(x, y), \quad (6b)$$

with $\mathcal{E} \equiv (E/\hbar v'_F \sqrt{\omega_B})^2$. Thus, we have two Schrödinger equations, each corresponding to a harmonic oscillator, but whose eigenvalues are related as

$$\mathcal{E}_{1,n-1} = \mathcal{E}_{2,n} = n, \quad n \geq 1, \quad \mathcal{E}_{2,0} = 0, \quad (7)$$

such that the energy spectrum turns out to be

$$E_n = \pm \hbar v'_F \sqrt{n \omega_B}, \quad n = 0, 1, 2, \dots, \quad (8)$$

where the positive (negative) energy corresponds to electrons in the conduction (valence) band. As a part of our discussion, we will just consider electrons in the conduction band.

Proceeding as in Ref. [35], the normalized eigenfunctions of the Hamiltonian \mathcal{H}^+ turn out to be [23]

$$\begin{aligned} \psi_{m,n}(\rho, \theta) = & (-1)^{\min(m,n)} \sqrt{\frac{\omega_B \min(m,n)!}{4\pi \max(m,n)!}} \left(\frac{\sqrt{\omega_B}}{2} \rho \right)^{|n-m|} \exp\left(-\frac{\omega_B}{8} \rho^2 + i(n-m)\theta\right) \times \\ & \times L_{\min(m,n)}^{|n-m|} \left(\frac{\omega_B}{4} \rho^2 \right), \end{aligned} \quad (9)$$

with $n, m = 0, 1, 2, \dots$ and $L_a^b(x)$ representing the associated Laguerre polynomials. Notice that the normalized eigenfunctions of the Hamiltonian \mathcal{H}^- are obtained simply as $\psi_{m,n-1} = A_\zeta^- \psi_{m,n}/\sqrt{n}$.

As we can see, the eigenstates of the Hamiltonians \mathcal{H}^\pm are labeled by two positive, integer numbers m, n , that correspond to the eigenvalues of two number operators M and N , respectively (see Appendix A):

$$\psi_1(\xi, \theta) \equiv \psi_{m,n-1}(\xi, \theta), \quad \psi_2(\xi, \theta) \equiv \psi_{m,n}(\xi, \theta). \quad (10)$$

From Eq. (A.5c), one concludes that the states $\psi_{m,n}$ are also eigenstates of the angular momentum-like operator $L_z = N - M$ with eigenvalue $m_z = n - m$.

Finally, by defining the z -component of the total angular momentum operator as $\mathbb{J}_z = L_z \otimes \mathbb{I} + \sigma_z/2$, we have that

$$\mathbb{J}_z \Psi_{m,n}(x, y) = \left(m_z - \frac{1}{2} \right) \Psi_{m,n}(x, y) = j \Psi_{m,n}(x, y), \quad (11)$$

i.e., the states $\Psi_{m,n}(x, y)$ are also eigenstates of \mathbb{J}_z with rational eigenvalue $j \equiv m_z - 1/2$.

In Appendix B, we establish a classification of the states $\Psi_{m,n}(x, y)$ according to the sign of m_z .

3 Annihilation operators

Let us define two independent annihilation operators \mathbb{A}_ζ^- and \mathbb{B}_ζ^- as

$$\mathbb{A}_\zeta^- = \begin{bmatrix} \cos(\delta) \frac{\sqrt{N+2}}{\sqrt{N+1}} A_\zeta^- & \sin(\delta) \frac{1}{\sqrt{N+1}} (A_\zeta^-)^2 \\ -\sin(\delta) \sqrt{N+1} & \cos(\delta) A_\zeta^- \end{bmatrix}, \quad (12a)$$

$$\mathbb{B}_\zeta^- = \begin{bmatrix} \cos(\eta) B_\zeta^- & \sin(\eta) \frac{B_\zeta^-}{\sqrt{N+1}} A_\zeta^- \\ -\sin(\eta) A_\zeta^+ \frac{B_\zeta^-}{\sqrt{N+1}} & \cos(\eta) B_\zeta^- \end{bmatrix}, \quad (12b)$$

such that $\delta, \eta \in [0, 2\pi]$ and for $m, n \in \mathbb{Z}^+ \cup \{0\}$:

$$\mathbb{A}_\zeta^- \Psi_{m,n}^\pm = \frac{\exp(i\delta)}{\sqrt{2^{\delta_{1n}}}} \sqrt{n} \Psi_{m,n-1}^\pm, \quad (13a)$$

$$\mathbb{B}_\zeta^- \Psi_{m,n}^\pm = \sqrt{m} \omega_n \Psi_{m-1,n}^\pm, \quad (13b)$$

with $\omega_n \equiv \cos(\eta) + i \sin(\eta)(1 - \delta_{0n})$.

Additionally, let us consider the following operator

$$\mathbb{K}_\zeta^- = \mathbb{A}_\zeta^- \mathbb{B}_\zeta^- \equiv \begin{bmatrix} \cos(\gamma) \frac{\sqrt{N+2}}{\sqrt{N+1}} A_\zeta^- B_\zeta^- & \sin(\gamma) \frac{1}{\sqrt{N+1}} (A_\zeta^-)^2 B_\zeta^- \\ -\sin(\gamma) \sqrt{N+1} B_\zeta^- & \cos(\gamma) A_\zeta^- B_\zeta^- \end{bmatrix}, \quad (14)$$

where $\gamma = \delta + \eta \in [0, 2\pi]$ —due to the periodicity of sine and cosine functions—such that for $m_z = 0, \pm 1, \pm 2, \dots$, it verifies

$$\mathbb{K}_\zeta^- \Phi_{m_z,n}^\pm = \frac{\exp(i\gamma)}{\sqrt{2^{\delta_{1n}}}} \sqrt{n(n - m_z)} \Phi_{m_z,n-1}^\pm, \quad (15)$$

for $n = 0, 1, 2, \dots$, with (see Fig. 2)

$$\Phi_{m_z,n}^\pm(x, y) = \frac{1}{\sqrt{2^{(1-\delta_{0n})}}} \begin{pmatrix} (1 - \delta_{0n}) \phi_{m_z-1,n-1}^\pm(x, y) \\ i \phi_{m_z,n}^\pm(x, y) \end{pmatrix}. \quad (16)$$

It is worth to remark that depending on the values of δ , η and γ , we can work with either diagonal or non-diagonal matrix operators.

On the other hand, bidimensional coherent states $\Psi_{\alpha,\beta}(x, y) \equiv \langle x, y | \alpha, \beta \rangle$ are defined as common eigenstates of the generalized annihilation operators \mathbb{A}_ζ^- and \mathbb{B}_ζ^- [26, 35, 36]:

$$\mathbb{A}_\zeta^- \Psi_{\alpha,\beta}(x, y) = \alpha \Psi_{\alpha,\beta}(x, y), \quad \alpha \in \mathbb{C}, \quad (17a)$$

$$\mathbb{B}_\zeta^- \Psi_{\alpha,\beta}(x, y) = \beta \Psi_{\alpha,\beta}(x, y), \quad \beta \in \mathbb{C}. \quad (17b)$$

Similarly, it is possible to construct another kind of coherent states, $\Phi_\tau^{m_z}(x, y) \equiv \langle x, y | \tau, m_z = n - m \rangle$ which are also eigenstates of the operator \mathbb{J}_z , *i.e.*,

$$\mathbb{K}_\zeta^- \Phi_\tau^{m_z}(x, y) = \tau \Phi_\tau^{m_z}(x, y), \quad \zeta \in \mathbb{C}, \quad (18a)$$

$$\mathbb{J}_z \Phi_\tau^{m_z}(x, y) = j \Phi_\tau^{m_z}(x, y), \quad j = \pm \frac{1}{2}, \pm \frac{3}{2}, \pm \frac{5}{2}, \dots \quad (18b)$$

A brief discussion regarding the algebras associated with these annihilation operators can be found in Appendix C. In the forthcoming sections, we build bidimensional and $su(1,1)$ coherent states [37–39] in graphene for some particular values of the parameters δ , η and γ .

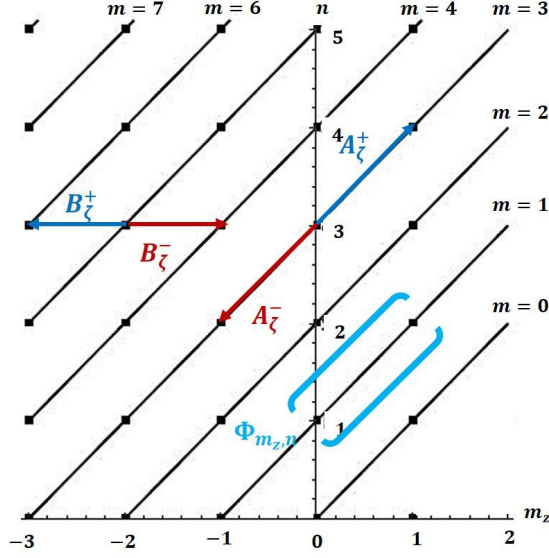


Figure 2: Space of scalar states $\phi_{m_z, n}$ is represented univocally by coordinates (m_z, n) . Inclined lines connect states with the value $m = n - m_z$. The plane is divided in two sectors according to $m_z \geq 0$ (right sector) or $m_z < 0$ (left sector).

3.1 Bidimensional coherent states (2D-CS)

In general, bidimensional states are a linear combination of all the stationary states $\Psi_{m, n}(x, y)$ [36]:

$$\Psi_{\alpha, \beta}(x, y) = \mathcal{N} \sum_{n=0}^{\infty} \sum_{m=0}^{\infty} c_n d_m \Psi_{m, n}(x, y) = \mathcal{N} \sum_{n=0}^{\infty} c_n \Psi_{\beta}^n(x, y) = \mathcal{N} \sum_{m=0}^{\infty} d_m \Psi_{\alpha}^m(x, y), \quad (19)$$

where \mathcal{N} is a normalization constant and the states $\Psi_{\alpha}^m(x, y)$, $\Psi_{\beta}^n(x, y)$ are the respective eigenstates of the operators \mathbb{A}_{ζ}^{-} and \mathbb{B}_{ζ}^{-} i.e.,

$$\begin{aligned} \mathbb{A}_{\zeta}^{-} \Psi_{\alpha}^m(x, y) &= \alpha \Psi_{\alpha}^m(x, y), \\ \mathbb{B}_{\zeta}^{-} \Psi_{\beta}^n(x, y) &= \beta \Psi_{\beta}^n(x, y). \end{aligned} \quad (20)$$

Therefore, Eq. (19) provides a way to obtain bidimensional coherent states building first either the states $\Psi_{\alpha}^m(x, y)$ or $\Psi_{\beta}^n(x, y)$ and then gathering them together properly (see Appendix D).

Hence, we obtain the explicit expression for the bidimensional coherent states

$$\Psi_{\alpha, \beta}(x, y) = \frac{\exp\left(\left[\beta - \frac{z}{2}\right] z^* - \frac{|\beta|^2}{2}\right)}{\sqrt{\pi(2 \exp(|\tilde{\alpha}|^2) - 1)}} \sum_{n=0}^{\infty} \frac{\tilde{\alpha}^n}{n!} \begin{pmatrix} \sqrt{n}(z - \beta)^{n-1} \\ i(z - \beta)^n \end{pmatrix}, \quad (21)$$

where z is given by Eq. (D.4) and $\tilde{\alpha} = \alpha \exp(-i\delta)$. It is straightforward to verify that these quantum states satisfy the eigenvalue equations in (17). Note that the δ -parameter introduces a phase factor to the eigenvalue α .

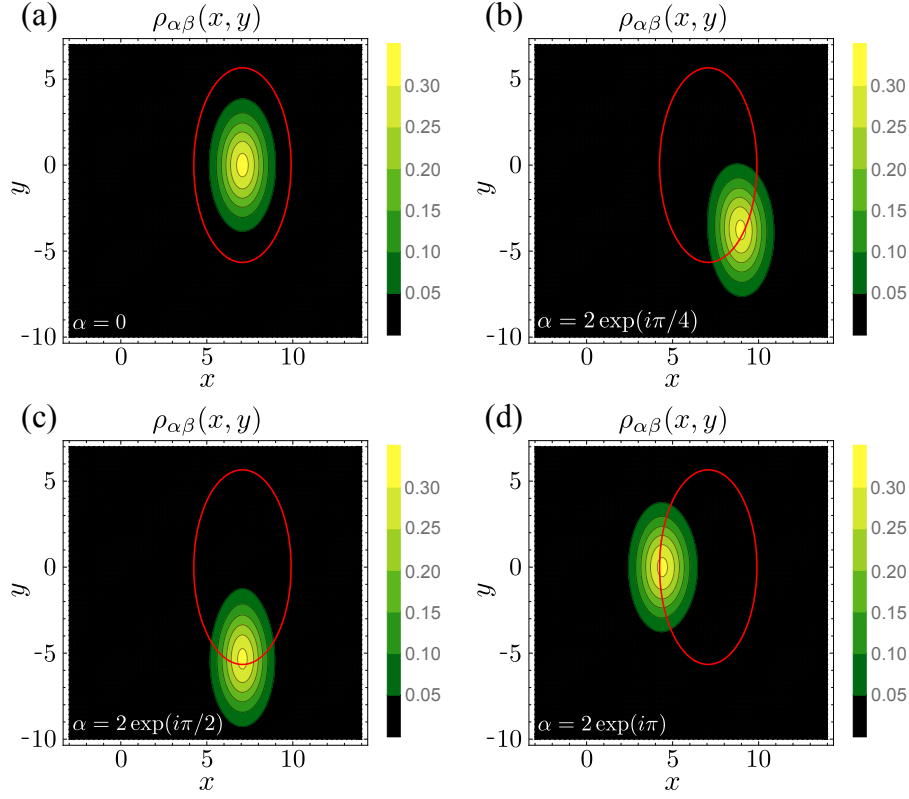


Figure 3: For the 2D-CS $\Psi_{\alpha,\beta}(x, y)$, the probability density $\rho_{\alpha,\beta}(x, y)$ is shown for some values of α . In all the cases $\beta = 5$, $B_0 = \zeta = 1/2$, $\delta = 0$ and $\omega_B = 1$. Red curves on the xy -plane describe the classical trajectory of a charge carrier in a magnetic field: the coordinates of the ellipse center are determined by β while α gives the coordinates in which the maximum probability amplitude can be found respect to that point.

Finally, the corresponding probability density $\rho_{\alpha,\beta}(x, y)$ and mean energy value $\langle H \rangle_\alpha$ are, respectively (see Figs. 3-5):

$$\begin{aligned} \rho_{\alpha,\beta}(x, y) &= \Psi_{\alpha,\beta}^\dagger(x, y) \Psi_{\alpha,\beta}(x, y) \\ &= \frac{\exp(-|z - \beta|^2)}{\pi(2 \exp(|\tilde{\alpha}|^2) - 1)} \left[1 + \left| \sum_{n=1}^{\infty} \frac{[\tilde{\alpha}(z - \beta)]^n}{n!} \right|^2 + \left| \sum_{n=1}^{\infty} \frac{[\tilde{\alpha}(z - \beta)]^n \sqrt{n}}{n!(z - \beta)} \right|^2 + 2\Re \left[\sum_{n=1}^{\infty} \frac{[\tilde{\alpha}(z - \beta)]^n}{n!} \right] \right], \end{aligned} \quad (22a)$$

$$\langle H \rangle_\alpha = \frac{2\sqrt{\omega_B} \hbar v'_F}{2 \exp(|\tilde{\alpha}|^2) - 1} \sum_{n=0}^{\infty} \frac{|\tilde{\alpha}|^{2n}}{n!} \sqrt{n}. \quad (22b)$$

Figures 3 and 4 show that the complex parameters α and β determine jointly where the maximum probability density is on the xy -plane. Moreover, the probability density $\rho_{\alpha,\beta}(x, y)$ exhibits a stable shape regardless of the value of α and β , so that the behavior of $\rho_{\alpha,\beta}(x, y)$ function resembles the squeezed coherent states (SCS) in phase space representation.

Also, as we can see, the eigenvalues α and $\beta = |\beta| \exp(i\varphi)$ are related with the geometric parameters of the classical elliptic trajectory of a charged particle in a magnetic field on the

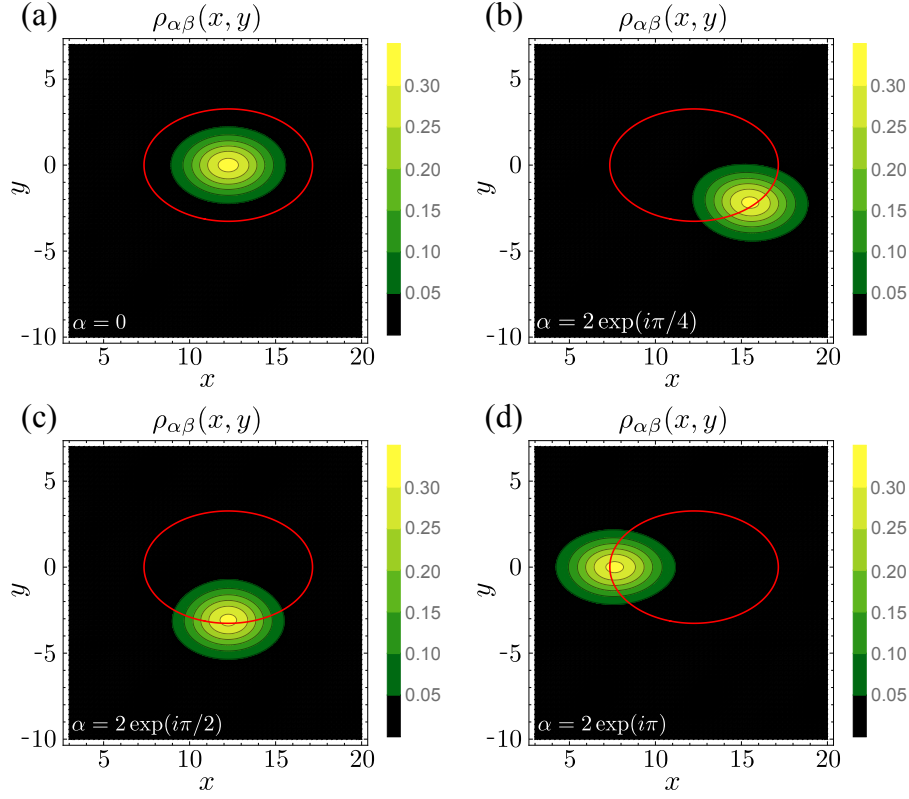


Figure 4: For the 2D-CS $\Psi_{\alpha,\beta}(x, y)$, the probability density $\rho_{\alpha,\beta}(x, y)$ is shown for some values of α . In all the cases $\beta = 5$, $B_0 = 1/2$, $\zeta = 3/2$, $\delta = 0$ and $\omega_B = 1$. Red curves on the xy -plane describe the classical trajectory of a charge carrier in a magnetic field: the coordinates of the ellipse center are determined by β while α gives the coordinates in which the maximum probability amplitude can be found respect to that point.

xy -plane (see again Figs. 3 and 4):

$$\frac{(x - x_0)^2}{4\zeta|\alpha|^2} + \frac{(y - y_0)^2}{4\zeta^{-1}|\alpha|^2} = 1, \quad (23)$$

where the points

$$(x_0, y_0) = \left(\frac{2\zeta^{1/2}|\beta|}{\sqrt{\omega_B}} \cos(\varphi), \frac{2\zeta^{-1/2}|\beta|}{\sqrt{\omega_B}} \sin(\varphi) \right), \quad (24)$$

determine the coordinates of the center of the curve respect to the origin $(0,0)$, while the eccentricity ε is given by

$$\varepsilon_x = \sqrt{1 - \zeta^2}, \quad \text{for } v_x < v_y, \quad (25a)$$

$$\varepsilon_y = \sqrt{1 - \zeta^{-2}}, \quad \text{for } v_x > v_y. \quad (25b)$$

Therefore, when the anisotropy is directed along the x -direction, the peak of maximum probability is found in elliptical curve whose semi-major axis is parallel to y -axis (Fig. 3), while if the

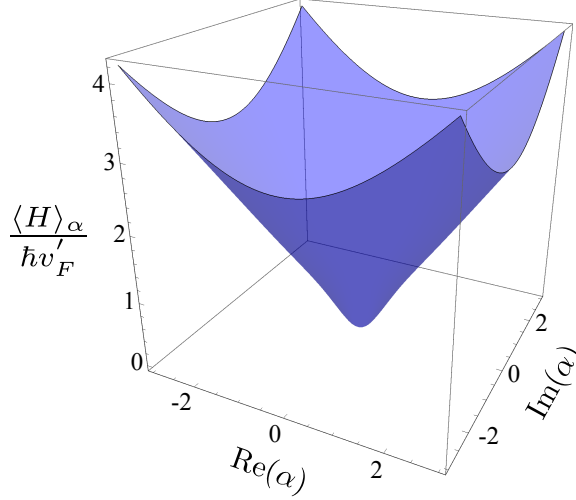


Figure 5: Mean energy $\langle H \rangle_\alpha / \hbar v'_F$ as a function of α with $B_0 = 1/2$ and $\omega_B = 1$.

anisotropy is along the y -direction, the semi-major axis is parallel to x -axis (Fig. 4). Moreover, for the isotropic case we have that $\zeta = 1$ and $\varepsilon_x = \varepsilon_y = 0$, *i.e.*, we obtain a probability density $\rho_{\alpha,\beta}(x, y)$ that has a Gaussian-like shape and whose maximum value is located in a circular curve.

3.2 $su(1,1)$ coherent states ($su(1,1)$ -CS)

Eq. (15) implies the states that are annihilated by the operator \mathbb{K}_ζ^- are those ones with the minimum energy values $E_0 = 0$ (for $m_z \leq 0$) and $E_{m_z} = \hbar v'_F \sqrt{m_z \omega}$ (for $m_z \geq 0$) (see Fig. 2). Thus, for a fixed value of m_z , any state can be expressed as a linear combination of states labeled as $\Psi_{m_z,n}(x, y)$:

$$\Phi^{m_z}(x, y) = \sum_{n=\max(0, m_z)}^{\infty} c_{m_z,n} \Phi_{m_z,n}(x, y), \quad (26)$$

$m_z = 0, \pm 1, \pm 2, \dots$, such that, under Eq. (11),

$$\mathbb{J}_z \Phi^{m_z}(x, y) = j \Phi^{m_z}(x, y), \quad j = m_z - \frac{1}{2}. \quad (27)$$

This means that the coherent states $\Phi_\tau^{m_z}(x, y)$ will have a defined angular momentum in z -direction (positive or negative sign) according to the sector to which the states $\Psi_{m_z,n}(x, y)$ that contribute to the superposition in Eq. (26) belong (right or left sector in Fig. 2).

As previous section, the states $\Phi_\tau^{m_z}(x, y)$ are obtained for the particular values $\eta = 0$ and $\gamma = \delta$ in Eq. (14).

For each sector in Fig. 2, the $su(1,1)$ -CS turn out to be, respectively:

$$\Phi_{\tau}^{m_z \geq 0}(x, y) = \frac{1}{\sqrt{{}_0F_1(; m_z + 1; |\tilde{\tau}|^2)}} \sum_{n=m_z}^{\infty} \frac{\sqrt{m_z!} \tilde{\tau}^{n-m_z}}{\sqrt{n!(n-m_z)!}} \Phi_{m_z, n}(x, y), \quad (28a)$$

$$\begin{aligned} \Phi_{\tau}^{m_z < 0}(x, y) &= \frac{1}{\sqrt{{}_2{}_0F_1(; -m_z + 1; |\tilde{\tau}|^2) - 1}} \times \\ &\times \left[\Phi_{m_z, 0}(x, y) + \sum_{n=1}^{\infty} \frac{\sqrt{2(-m_z)!} \tilde{\tau}^n}{\sqrt{n!(n-m_z)!}} \Phi_{m_z, n}(x, y) \right], \end{aligned} \quad (28b)$$

where $\tilde{\tau} = \tau \exp(-i\delta)$ and ${}_pF_q$ is a generalized hypergeometric function defined by

$${}_pF_q(a_1, \dots, a_p, b_1, \dots, b_q; x) = \sum_{n=0}^{\infty} \frac{(a_1)_n \cdots (a_p)_n}{(b_1)_n \cdots (b_q)_n} \frac{x^n}{n!}, \quad (29)$$

where $(a)_k$ is the Pochhammer symbol,

$$(a)_k = \frac{\Gamma(a+k)}{\Gamma(a)}. \quad (30)$$

The corresponding probability and mean energy value are given by (see Figs. 6-8):

$$\begin{aligned} \rho_{m_z, \tau}(x, y) &= \rho_{m_z, \tau}(\xi) = \Phi_{\tau}^{m_z \dagger}(x, y) \Phi_{\tau}^{m_z}(x, y) = \frac{\omega_B |z|^{2m_z} \exp(-\xi^2)}{8\pi [{}_0F_1(; m_z + 1; |\tilde{\tau}|^2)]} \times \\ &\times \left[\left| \sum_{n=m_z}^{\infty} \frac{\sqrt{m_z!} (-\tilde{\tau})^{n-m_z}}{n!} L_{n-m_z}^{m_z}(\xi^2) \right|^2 + \left| \sum_{n=m_z}^{\infty} \frac{\sqrt{m_z!} (-\tilde{\tau})^{n-m_z} z^{-1}}{\sqrt{n(n-1)!}} L_{n-m_z}^{m_z-1}(\xi^2) \right|^2 \right], \end{aligned} \quad (31a)$$

$$\langle H \rangle_{\tau} = \frac{\sqrt{\omega_B} \hbar v'_F}{{}_0F_1(; m_z + 1; |\tilde{\tau}|^2)} \sum_{n=m_z}^{\infty} \frac{m_z! |\tilde{\tau}|^{2n-2m_z}}{n!(n-m_z)!} \sqrt{n}, \quad \text{for } m_z \geq 0, \quad (31b)$$

$$\begin{aligned} \rho_{m_z, \tau}(x, y) &= \rho_{m_z, \tau}(\xi) = \Phi_{\tau}^{m_z \dagger}(x, y) \Psi_{\tau}^{m_z}(x, y) = \frac{\omega_B |z|^{-2m_z} \exp(-\xi^2)}{4\pi [{}_2{}_0F_1(; -m_z + 1; |\tilde{\tau}|^2) - 1]} \times \\ &\times \left[\frac{1}{(-m_z)!} + \left| \sum_{n=1}^{\infty} \frac{\sqrt{(-m_z)!} (-\tilde{\tau})^n}{(n-m_z)!} L_n^{-m_z}(\xi^2) \right|^2 + \left| \sum_{n=1}^{\infty} \frac{\sqrt{(-m_z)!} (-\tilde{\tau})^n}{(n-m_z)!} \frac{z}{\sqrt{n}} L_{n-1}^{-m_z+1}(\xi^2) \right|^2 \right] \\ &+ 2\Re \left[\sum_{n=1}^{\infty} \frac{(-\tilde{\tau})^n}{(n-m_z)!} L_n^{-m_z}(\xi^2) \right], \end{aligned} \quad (31c)$$

$$\langle H \rangle_{\tau} = \frac{2\sqrt{\omega_B} \hbar v'_F}{{}_2{}_0F_1(; -m_z + 1; |\tilde{\tau}|^2) - 1} \sum_{n=0}^{\infty} \frac{(-m_z)! |\tilde{\tau}|^{2n}}{n!(n-m_z)!} \sqrt{n}, \quad \text{for } m_z \leq 0. \quad (31d)$$

Figures 6 and 7 show that the probability density of the $su(1,1)$ coherent states (with both positive and negative z -component of the total angular momentum operator) always stays

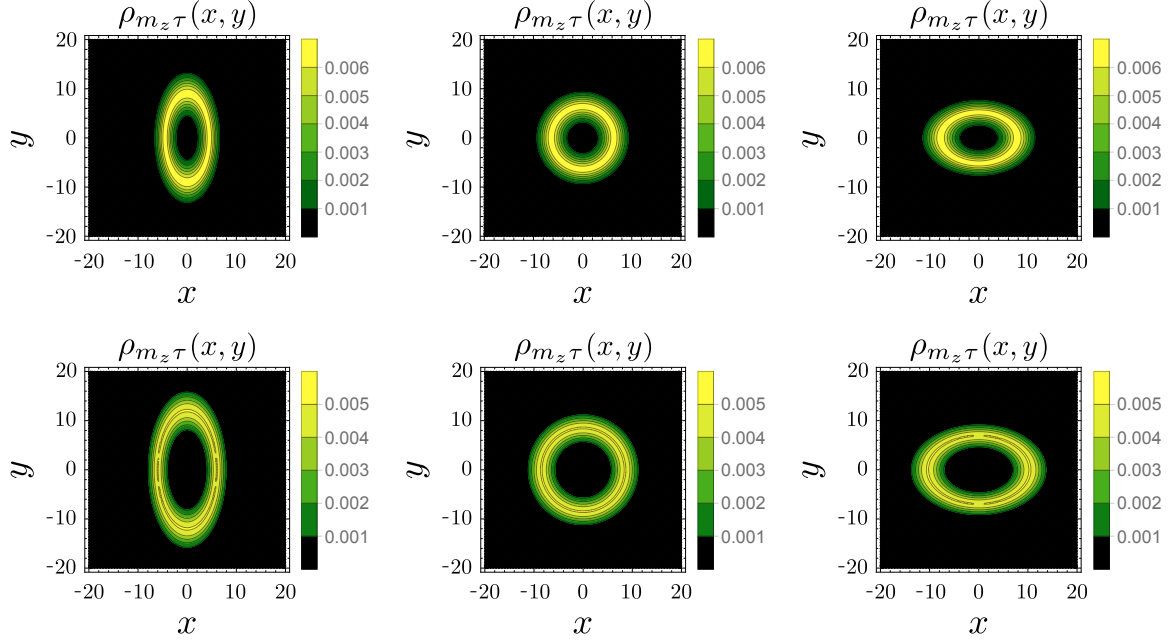


Figure 6: Probability density $\rho_{m_z,\tau}(x, y)$ for the coherent states in Eq. (28a) with $|j| = 1/2$ for different values of the ζ -parameter and $|\tau|$ -eigenvalue: (vertical) $\zeta = 1/2, 1, 3/2$, and (horizontal) $|\tau| = 3, 5$. In all these cases $B_0 = 1/2$, $\omega_B = 1$ and $\delta = 0$.

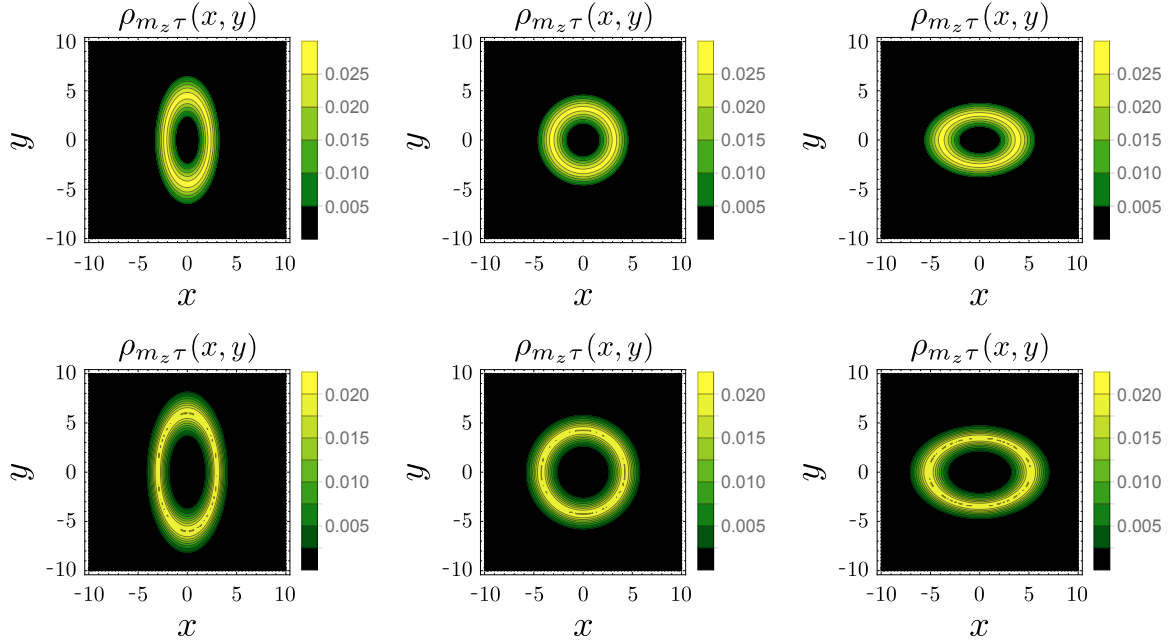


Figure 7: Probability density $\rho_{m_z,\tau}(x, y)$ for the coherent states in Eq. (28b) with $|j| = 3/2$ for different values of the ζ -parameter and $|\tau|$ -eigenvalue: (vertical) $\zeta = 1/2, 1, 3/2$, and (horizontal) $|\tau| = 3, 5$. In all these cases $B_0 = 2$, $\omega_B = 2$ and $\delta = 0$.

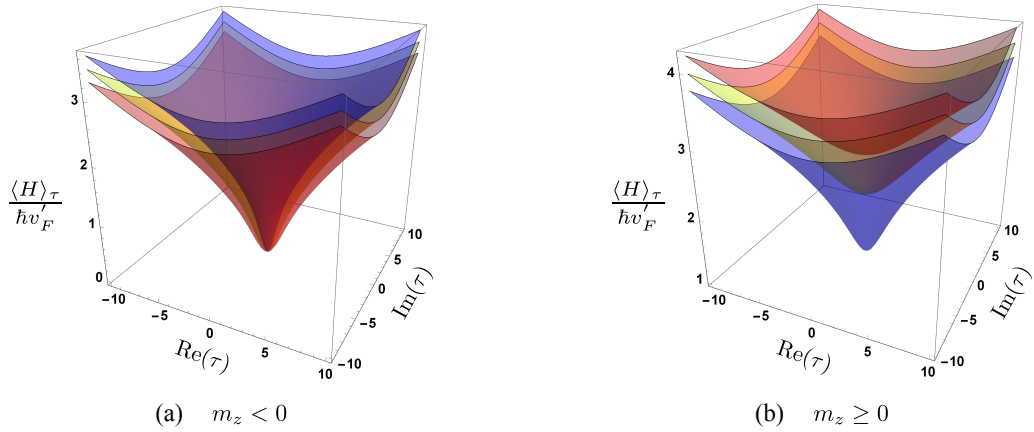


Figure 8: Mean energy value $\langle H \rangle_\tau / \hbar v'_F$ as a function of τ for the $su(1,1)$ -CS $\Phi_\tau^{m_z}(x, y)$ with $|m_z| = 1$ (blue), $|m_z| = 4$ (yellow) and $|m_z| = 7$ (red). In all the cases $B_0 = 1/2$, $\omega_B = 1$ and $\delta = 0$.

centered at the origin for any value of the eigenvalue τ , in contrast to the bidimensional coherent states for which their eigenvalues α and β determine the location of the maximum probability density on the xy -plane. However, for a given magnetic field strength and ζ -value, both τ and m_z (or j) modify the probability density: as the parameters $|\tau|$ and $|j|$ increase, the maximum probability moves away radially from the origin following the criterion given in Eq. (25). Besides, if the magnetic field strength increases, the maximum probability also does while the distance respect to origin decreases following the elliptical shape adopted, which is according to the semi-classical behavior of charged particle in a magnetic field.

On the other hand, as the z -component of the total angular momentum $|j|$ increases, for coherent states with $j < 0$ the corresponding mean energy $\langle H \rangle_\tau$ takes values becoming smaller; meanwhile, for the states with $j > 0$ the contrary effect occurs (see Fig. 8).

4 Final remarks

In this work, in order to analyze the bidimensional effects of the anisotropy in 2D-Dirac materials on the dynamics of their charge carriers, we have obtained bidimensional and $su(1,1)$ coherent states through a symmetric gauge vector potential for the interaction between such particles and a homogeneous orthogonal magnetic field. Such coherent states have been obtained as eigenstates of generalized annihilation operators that satisfy either the Heisenberg-Weyl or $su(1,1)$ algebras.

For the vector potential in Eq. (1), energy spectrum of the anisotropic Dirac Hamiltonian H has an infinite degeneracy due to the rotational symmetry, $[\mathcal{H}^\pm, L_z] = 0$, while its solutions have axial-like symmetry (Eq. (B.1)). Moreover, we can identify two set of scalar ladder operators that satisfy two independent copies of the Heisenberg-Weyl algebra and with which, it is possible to define a set of generalized annihilation operators \mathbb{A}_ζ^- , \mathbb{B}_ζ^- and \mathbb{K}_ζ^- (Eqs. (12a, 12b and 14). By employing these annihilation operators, at least two different kinds of coherent states $\Psi_{\alpha,\beta}(x, y)$

and $\Phi_\tau^{m_z}(x, y)$ are obtained, each one with different characteristics.

The first family of coherent states, identified as 2D-CS $\Psi_{\alpha,\beta}(x, y)$, exhibits a stable shape for any value of the eigenvalues α and β (Fig. 3), which determine the location of the maximum probability peak. In addition, Figure 4 shows the anisotropy effect on these states: as ζ -parameter grows, *i.e.*, we go from a Dirac cone aligned to the p_x -direction to one aligned to the p_y -direction, the probability density is aligned from being parallel to the y -axis to being parallel to x -axis, acquiring an elliptical or circular projection over the xy -plane. When $\zeta = 1$, one recovers the results in Ref. [34], so we can consider those ones as a particular case of the coherent states here presented. Likewise, the second family or $su(1,1)$ -CS $\Phi_\tau^{m_z}(x, y)$ possesses a probability distribution whose shape is basically an elliptical ring around the origin of coordinates (Figs. 6 and 7), and whose length of the semi-major axis depends on the value of the ζ -parameter. Once again, changing the anisotropy direction, charge carriers are *confined* to move in one or another direction, that along with a growing magnetic field strength, the probability to find such particles in a particular region on the xy -plane also increases.

In addition, the behavior of the mean energy values (Figs. 5 and 8) suggests the possibility of using both families of coherent states in graphene in semi-classical treatments. Besides, in the limit $\alpha \rightarrow 0$ and $\tau \rightarrow 0$, the $\langle H \rangle_\alpha$ and $\langle H \rangle_\tau$ functions behave differently, as we can see in Figs. 5 and 8. This is due to that the minimum energy states that contribute to both superpositions in Eqs. (21) and (28a) are those ones with $E_0 = 0$, while that for the linear combination in Eq. (28b) are excited states with $E_n = \hbar v'_F \sqrt{m_z \omega}$.

Finally, we would like to empathize that since 2D-CS and $su(1,1)$ -CS obtained here describe the same physical problem, they share information that expresses in a different way. For instance, the corresponding probability densities are deformed, showing an elliptically *squeezed* distribution for the former and elliptical ring for the latter, which is according with the ζ -parameter that depends on the anisotropy in 2D-DM. Likewise, the main difference between them is the bidimensional coherent states allow to describe the probability of finding an electron in a small section of a closed trajectory but knowing nothing about the z -component of the total angular momentum, while with the $su(1,1)$ coherent states one can find the particle along the whole elliptical curve with equal probability but having meaningful information about the z -component of the total angular momentum. These facts become useful 2D-CS and $su(1,1)$ -CS to calculate some experimental physical quantities for which such quantum states could give information from a semi-classical approach.

Acknowledgments

YCS acknowledges support from CIC-UMSNH under grant 3820801. AR acknowledges support from Consejo Nacional de Ciencia y Tecnología (México) under grant 256494. EDB acknowledges IFM-UMSNH for its warm hospitality.

A Algebraic structure and eigenstates

In order to obtain the algebraic relations associated to this system, we make the following coordinate transformation

$$x = \zeta^{1/2} \rho \cos(\theta), \quad y = \zeta^{-1/2} \rho \sin(\theta), \quad (\text{A.1})$$

that corresponds to the ellipse equation

$$\frac{x^2}{\zeta \rho^2} + \frac{y^2}{\zeta^{-1} \rho^2} = 1. \quad (\text{A.2})$$

Thus, by defining the dimensionless variable ξ as

$$\xi = \frac{\sqrt{\omega_B}}{2} \rho, \quad (\text{A.3})$$

the corresponding Hamiltonian operators in Eq. (6) [23, 25, 35] can be factorized in terms of two sets of differential operators, namely [35, 40, 41],

$$\mathcal{H}^+ = A_\zeta^+ A_\zeta^- = B_\zeta^+ B_\zeta^- + L_z, \quad \mathcal{H}^- = \mathcal{H}^+ + 1, \quad (\text{A.4})$$

where

$$A_\zeta^- = \frac{\exp(-i\theta)}{2} \left(\partial_\xi - \frac{i\partial_\theta}{\xi} + \xi \right), \quad A_\zeta^+ = (A_\zeta^-)^\dagger, \quad (\text{A.5a})$$

$$B_\zeta^- = \frac{\exp(i\theta)}{2} \left(\partial_\xi + \frac{i\partial_\theta}{\xi} + \xi \right), \quad B_\zeta^+ = (B_\zeta^-)^\dagger, \quad (\text{A.5b})$$

$$L_z = -i\partial_\theta = N - M, \quad (\text{A.5c})$$

being $L_z = (\zeta^{-1} x p_y - \zeta y p_x) / \hbar$ the z -component of an angular momentum-like operator and $N = A_\zeta^+ A_\zeta^-$ and $M = B_\zeta^+ B_\zeta^-$ are number operators. The above operators satisfy the following commutation relations

$$[A_\zeta^-, A_\zeta^+] = \mathbf{1}, \quad [B_\zeta^-, B_\zeta^+] = \mathbf{1}, \quad (\text{A.6a})$$

$$[A_\zeta^\pm, B_\zeta^\pm] = \mathbf{0}, \quad [A_\zeta^\pm, B_\zeta^\mp] = \mathbf{0}, \quad (\text{A.6b})$$

$$[L_z, A_\zeta^\pm] = \pm A_\zeta^\pm, \quad [L_z, B_\zeta^\pm] = \mp B_\zeta^\pm. \quad (\text{A.6c})$$

These relationships imply that each set of ladder operators A_ζ^\pm and B_ζ^\pm are generators of the Heisenberg-Weyl algebra and are also independent of each other.

Eq. (A.6c) implies that the operators A_ζ^+ and A_ζ^- , upon acting on an eigenstate of L_z , increase or decrease, respectively, the eigenvalue of L_z in an unity; meanwhile, the operators B_ζ^\pm have the contrary effect.

In addition, the action of the operators A_ζ^\pm and B_ζ^\pm on the states $\psi_{m,n}$ is (see Fig. 9)

$$A_\zeta^- \psi_{m,n} = \sqrt{n} \psi_{m,n-1}, \quad A_\zeta^+ \psi_{m,n} = \sqrt{n+1} \psi_{m,n+1}, \quad (\text{A.7a})$$

$$B_\zeta^- \psi_{m,n} = \sqrt{m} \psi_{m-1,n}, \quad B_\zeta^+ \psi_{m,n} = \sqrt{m+1} \psi_{m+1,n}. \quad (\text{A.7b})$$

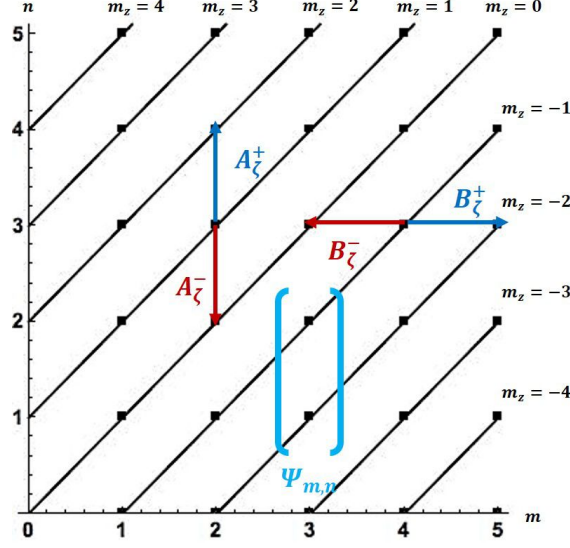


Figure 9: Space of scalar states $\psi_{m,n}$ is represented univocally by coordinates (m, n) . Inclined lines connect states with the same angular momentum $m_z = n - m$. The plane is divided in two sectors according to $m_z \geq 0$ (upper sector) or $m_z \leq 0$ (lower sector).

B Classification of eigenstates

We can label as $\Psi_{m,n}^+(x, y)$ the spinor states whose two scalar components have positive z -component of the angular momentum ($m_z \geq 0$), and as $\Psi_{m,n}^-(x, y)$ those ones whose two scalar components have negative z -component angular momentum ($m_z \leq 0$), *i.e.*,

$$\Psi_{m,n}^+(x, y) = \frac{1}{\sqrt{2}} \begin{pmatrix} \psi_{m,n-1}^+(x, y) \\ i\psi_{m,n}^+(x, y) \end{pmatrix}, \quad (\text{B.1a})$$

$$\Psi_{m,n}^-(x, y) = \frac{1}{\sqrt{2(1-\delta_{0n})}} \begin{pmatrix} (1 - \delta_{0n})\psi_{m,n-1}^-(x, y) \\ i\psi_{m,n}^-(x, y) \end{pmatrix}, \quad (\text{B.1b})$$

where $\psi_{m,n}^+(x, y) \equiv \psi_{m,n}^+(\rho, \theta)$ ($\psi_{m,n}^-(x, y) \equiv \psi_{m,n}^-(\rho, \theta)$) identifies the states that belong to the upper (lower) sector in Fig. 9, and δ_{mn} denotes the Kronecker delta.

C Algebra generated by matrix operators

The operators \mathbb{A}_ζ^- and \mathbb{B}_ζ^- satisfy two independent copies of the Heisenberg-Weyl algebra:

$$[\mathbb{A}_\zeta^-, \mathbb{A}_\zeta^+] = \mathbb{I}, \quad \mathbb{A}_\zeta^+ = (\mathbb{A}_\zeta^-)^\dagger, \quad (\text{C.1a})$$

$$[\mathbb{B}_\zeta^-, \mathbb{B}_\zeta^+] = \mathbb{I}, \quad \mathbb{B}_\zeta^+ = (\mathbb{B}_\zeta^-)^\dagger, \quad (\text{C.1b})$$

$$[\mathbb{A}_\zeta^\pm, \mathbb{B}_\zeta^\pm] = [\mathbb{A}_\zeta^\pm, \mathbb{B}_\zeta^\mp] = \mathbf{0}. \quad (\text{C.1c})$$

Likewise, considering $\mathbb{K}_\zeta^+ = (\mathbb{K}_\zeta^-)^\dagger$, we get

$$[\mathbb{K}_\zeta^-, \mathbb{K}_\zeta^+] = 2\mathbb{K}_\zeta = \begin{bmatrix} N + M + 2 & 0 \\ 0 & N + M + 1 \end{bmatrix}, \quad (\text{C.2a})$$

$$[\mathbb{K}_\zeta, \mathbb{K}_\zeta^\pm] = \pm \mathbb{K}_\zeta^\pm. \quad (\text{C.2b})$$

which allow us to identify an $su(1, 1)$ algebra.

D Obtaining the 2D-CS

In order to obtain the simplest form for bidimensional coherent states, we proceed to build the states $\Psi_\beta^n(x, y)$ for the case with $\eta = 0$, so that $\mathbb{B}_\zeta^- = B_\zeta^- \otimes \mathbb{I}$. From the corresponding eigenvalue equation (20), the coherent states $\Psi_\beta^n(x, y)$ turn out to be

$$\Psi_\beta^n(x, y) = \frac{1}{\sqrt{2^{(1-\delta_{0n})}}} \begin{pmatrix} (1 - \delta_{0n})\psi_\beta^{n-1}(x, y) \\ i\psi_\beta^n(x, y) \end{pmatrix}, \quad (\text{D.1})$$

where $\psi_\beta^n(x, y)$ and $\psi_\beta^{n-1}(x, y)$ are identified as scalar eigenstates of the operator B_ζ^- for each n index, *i.e.*, these states are stationary with a well-defined energy E_n .

Now, one can notice that each of these coherent states satisfies one of the following equation systems,

$$\begin{cases} B_\zeta^- \psi_\beta^n = \beta \psi_\beta^n, \\ A_\zeta^+ A_\zeta^- \psi_\beta^n = n \psi_\beta^n, \end{cases} \quad \begin{cases} B_\zeta^- \psi_\beta^{n-1} = \beta \psi_\beta^{n-1}, \\ A_\zeta^- A_\zeta^+ \psi_\beta^{n-1} = n \psi_\beta^{n-1}. \end{cases} \quad (\text{D.2})$$

Thus, after solving the systems of equations (D.2), the normalized coherent states $\Psi_\beta^n(x, y)$, $n = 0, 1, 2, \dots$, are

$$\Psi_\beta^n(x, y) = \frac{1}{\sqrt{2^{(1-\delta_{0n})} \pi n!}} \exp \left(\left[\beta - \frac{z}{2} \right] z^* - \frac{|\beta|^2}{2} \right) \begin{pmatrix} \sqrt{n}(z - \beta)^{n-1} \\ i(z - \beta)^n \end{pmatrix}, \quad (\text{D.3})$$

where the complex parameter z is defined by

$$z = \frac{\sqrt{\omega_B}}{2} (\zeta^{-1/2} x + i\zeta^{1/2} y) = \frac{\sqrt{\omega_B}}{2} \rho \exp(i\theta). \quad (\text{D.4})$$

Finally, by taking the sum over the n index, one gets the expression in (21).

E Completeness relation

We investigate the non-orthogonality property and the resolution of unity of both the bidimensional and $su(1, 1)$ coherent states.

First, the coherent states in Eq. (21) can be also rewritten, in Dirac notation, as

$$|\Psi_{\alpha, \beta}\rangle = \frac{\exp \left(-\frac{|\beta|^2}{2} \right)}{\sqrt{2 \exp(|\tilde{\alpha}|^2) - 1}} \left[\sum_{m=0}^{\infty} \frac{\beta^m}{\sqrt{m!}} |\Psi_{m,0}\rangle + \sum_{n=1}^{\infty} \sum_{m=0}^{\infty} \frac{\sqrt{2} \alpha^n \beta^m}{\sqrt{n!m!}} |\Psi_{m,n}\rangle \right]. \quad (\text{E.1})$$

Taking the inner product between two 2D-CS with different eigenvalues, we have that:

$$|\langle \Psi_{\alpha', \beta'} | \Psi_{\alpha, \beta} \rangle| = \left| \exp\left(-\frac{|\beta'|^2}{2}\right) \exp\left(-\frac{|\beta|^2}{2}\right) \frac{(2 \exp(\tilde{\alpha}'^* \tilde{\alpha}) - 1) \exp(\beta'^* \beta)}{\sqrt{2 \exp(|\tilde{\alpha}'|^2) - 1} \sqrt{2 \exp(|\tilde{\alpha}|^2) - 1}} \right|, \quad (\text{E.2})$$

which implies the non-orthogonality property of the 2D-CS. For $\alpha = \alpha'$ and $\beta = \beta'$, one recovers the normalization relationship $\langle \Psi_{\alpha, \beta} | \Psi_{\alpha, \beta} \rangle = 1$.

Now, choosing the measure

$$d\mu(\alpha, \beta) = \frac{2 \exp(|\tilde{\alpha}|^2) - 1}{2\pi^2} |\tilde{\alpha}| |\beta| e^{-|\tilde{\alpha}|^2} d|\tilde{\alpha}| d|\beta| d\theta d\varphi, \quad (\text{E.3})$$

it follows that

$$\begin{aligned} & \sum_{m=0}^{\infty} \frac{|\Psi_{m,0}\rangle \langle \Psi_{m,0}|}{2} + \int_{\mathbb{C}_\alpha} \int_{\mathbb{C}_\beta} |\Psi_{\alpha, \beta}\rangle \langle \Psi_{\alpha, \beta}| d\mu(\alpha, \beta) = \sum_{m=0}^{\infty} \frac{|\Psi_{m,0}\rangle \langle \Psi_{m,0}|}{2} + \int_{\mathbb{C}_\alpha} \int_{\mathbb{C}_\beta} \frac{d\mu(\alpha, \beta) \exp(-|\beta|^2)}{2 \exp(|\tilde{\alpha}|^2) - 1} \\ & \times \left[\sum_{m=0}^{\infty} \frac{\beta^m}{\sqrt{m!}} |\Psi_{m,0}\rangle + \sum_{n=1}^{\infty} \sum_{m=0}^{\infty} \frac{\sqrt{2} \alpha^n \beta^m}{\sqrt{n! m!}} |\Psi_{m,n}\rangle \right] \left[\sum_{m'=0}^{\infty} \frac{\beta^{*m'}}{\sqrt{m'!}} \langle \Psi_{m',0}| + \sum_{n'=1}^{\infty} \sum_{m'=0}^{\infty} \frac{\sqrt{2} \alpha^{*n'} \beta^{*m'}}{\sqrt{n'! m'!}} \langle \Psi_{m',n'}| \right] \\ & = \sum_{m=0}^{\infty} \frac{|\Psi_{m,0}\rangle \langle \Psi_{m,0}|}{2} + \frac{1}{2} \sum_{m=0}^{\infty} \int_0^\infty \frac{t^m e^{-t}}{m!} dt \int_0^\infty \left[|\Psi_{m,0}\rangle \langle \Psi_{m,0}| + 2 \sum_{n=1}^{\infty} \frac{|\Psi_{m,n}\rangle \langle \Psi_{m,n}|}{n!} s^n \right] e^{-s} ds \\ & = \sum_{m=0}^{\infty} \frac{|\Psi_{m,0}\rangle \langle \Psi_{m,0}|}{2} + \sum_{m=0}^{\infty} \frac{|\Psi_{m,0}\rangle \langle \Psi_{m,0}|}{2} + \sum_{n=1}^{\infty} \sum_{m=0}^{\infty} |\Psi_{m,n}\rangle \langle \Psi_{m,n}| \\ & = \sum_{m=0}^{\infty} |\Psi_{m,0}\rangle \langle \Psi_{m,0}| + \sum_{n=1}^{\infty} \sum_{m=0}^{\infty} |\Psi_{m,n}\rangle \langle \Psi_{m,n}| = \mathbf{1}, \end{aligned} \quad (\text{E.4})$$

where $t = |\beta|^2$, $s = |\tilde{\alpha}|^2$ and we use the following results

$$\int_0^{2\pi} \exp(i(p-q)\chi) d\chi = 2\pi \delta_{pq}, \quad (\text{E.5a})$$

$$\int_0^\infty x^k e^{-x} dx = \Gamma(k+1) = k!. \quad (\text{E.5b})$$

On the other hand, the $su(1,1)$ -CS with $j > 0$ in Eq. (28a) are expressed in Dirac notation as

$$|\Phi_\tau^{m_z}\rangle = \frac{1}{\sqrt{{}_0F_1(; m_z + 1; |\tilde{\tau}|^2)}} \sum_{n=m_z}^{\infty} \frac{\sqrt{m_z!} \tilde{\tau}^{n-m_z}}{\sqrt{n!(n-m_z)!}} |\Phi_{m_z, n}\rangle. \quad (\text{E.6})$$

The inner product of two coherent states with different eigenvalues turns out to be:

$$|\langle \Phi_{\tau'}^{m_z} | \Phi_\tau^{m_z} \rangle| = \left| \frac{{}_0F_1(; m_z + 1; \tilde{\tau}'^* \tilde{\tau})}{\sqrt{{}_0F_1(; m_z + 1; |\tilde{\tau}'|^2) {}_0F_1(; m_z + 1; |\tilde{\tau}|^2)}} \right|. \quad (\text{E.7})$$

This expression indicates the non-orthogonality property of the $su(1,1)$ -CS. When $\tau = \tau'$, we obtain again the normalization condition $\langle \Phi_\tau^{m_z} | \Phi_\tau^{m_z} \rangle = 1$.

Now, considering the measure

$$d\mu(\tau) = \frac{{}_0F_1(; m_z + 1; |\tilde{\tau}|^2)}{\pi} f(|\tilde{\tau}|) |\tilde{\tau}| d|\tilde{\tau}| d\theta, \quad (\text{E.8})$$

we get for a m_z given:

$$\begin{aligned} \int_{\mathbb{C}} |\Phi_{\tau}^{m_z}\rangle \langle \Phi_{\tau}^{m_z}| d\mu(\tau) &= \int_{\mathbb{C}} \frac{d\mu(\tilde{\tau})}{{}_0F_1(; m_z + 1; |\tilde{\tau}|^2)} \left[\sum_{n=m_z}^{\infty} \frac{\sqrt{m_z!} \tilde{\tau}^{n-m_z}}{\sqrt{n!(n-m_z)!}} |\Phi_{m_z, n}\rangle \right] \left[\sum_{n'=m_z}^{\infty} \frac{\sqrt{m_z!} \tilde{\tau}^{*n'-m_z}}{\sqrt{n'!(n'-m_z)!}} \langle \Phi_{m_z, n'}| \right] \\ &= \sum_{n=m_z}^{\infty} \frac{m_z! |\Phi_{m_z, n}\rangle \langle \Phi_{m_z, n}|}{n!(n-m_z)!} \int_0^{\infty} t^{n-m_z} f(t) dt \\ &= \sum_{n=m_z}^{\infty} |\Phi_{m_z, n}\rangle \langle \Phi_{m_z, n}| = \mathbf{1}_{m_z}, \end{aligned} \quad (\text{E.9})$$

where $t = |\tilde{\tau}|^2$ and $f(t)$ is a function that must satisfy

$$\int_0^{\infty} t^{n-m_z} f(t) dt = \frac{\Gamma(n+1)\Gamma(n-m_z+1)}{\Gamma(m_z+1)}. \quad (\text{E.10})$$

Finally, the $su(1, 1)$ -CS with $j < 0$ in Eq. (28b) read now as

$$|\Phi_{\tau}^{m_z}\rangle = \frac{1}{\sqrt{{}_2F_1(-m_z+1; |\tilde{\tau}|^2) - 1}} \left[|\Phi_{m_z, 0}\rangle + \sum_{n=1}^{\infty} \frac{\sqrt{2(-m_z)!} \tilde{\tau}^n}{\sqrt{n!(n-m_z)!}} |\Phi_{m_z, n}\rangle \right], \quad (\text{E.11})$$

whose inner product between CS with different eigenvalues is

$$|\langle \Phi_{\tau'}^{m_z} | \Phi_{\tau}^{m_z} \rangle| = \left| \frac{{}_2F_1(-m_z+1; \tilde{\tau}'^* \tilde{\tau}) - 1}{\sqrt{{}_2F_1(-m_z+1; |\tilde{\tau}'|^2) - 1} \sqrt{{}_2F_1(-m_z+1; |\tilde{\tau}|^2) - 1}} \right|. \quad (\text{E.12})$$

Once again, this expression indicates the non-orthogonality property of the corresponding $su(1, 1)$ -CS and the normalization condition $\langle \Phi_{\tau}^{m_z} | \Phi_{\tau}^{m_z} \rangle = 1$ is obtained for $\tau = \tau'$.

Assuming the following measure

$$d\mu(\tau) = \frac{{}_2F_1(-m_z+1; |\tilde{\tau}|^2) - 1}{2\pi} g(|\tilde{\tau}|) |\tilde{\tau}| d|\tilde{\tau}| d\theta, \quad (\text{E.13})$$

we have that

$$\begin{aligned} \frac{|\Phi_{m_z, 0}\rangle \langle \Phi_{m_z, 0}|}{2} + \int_{\mathbb{C}} |\Phi_{\tau}^{m_z}\rangle \langle \Phi_{\tau}^{m_z}| d\mu(\tau) &= \frac{|\Phi_{m_z, 0}\rangle \langle \Phi_{m_z, 0}|}{2} + \int_{\mathbb{C}} \frac{d\mu(\alpha)}{{}_2F_1(-m_z+1; |\tilde{\tau}|^2) - 1} \\ &\times \left[|\Phi_{m_z, 0}\rangle + \sum_{n=1}^{\infty} \frac{\sqrt{2(-m_z)!} \tilde{\tau}^n}{\sqrt{n!(n-m_z)!}} |\Phi_{m_z, n}\rangle \right] \left[\langle \Phi_{m_z, 0}| + \sum_{n'=1}^{\infty} \frac{\sqrt{2(-m_z)!} \tilde{\tau}^{*n'}}{\sqrt{n'!(n'-m_z)!}} \langle \Phi_{m_z, n'}| \right] \end{aligned} \quad (\text{E.14})$$

$$\begin{aligned}
&= \frac{|\Phi_{m_z,0}\rangle\langle\Phi_{m_z,0}|}{2} + \int_0^\infty \left[\frac{|\Phi_{m_z,0}\rangle\langle\Phi_{m_z,0}|}{2} + \sum_{n=1}^\infty \frac{(-m_z)!}{n!(n-m_z)!} |\Phi_{m_z,n}\rangle\langle\Phi_{m_z,n}| t^n \right] g(t) dt \\
&= \frac{|\Phi_{m_z,0}\rangle\langle\Phi_{m_z,0}|}{2} + \frac{|\Phi_{m_z,0}\rangle\langle\Phi_{m_z,0}|}{2} \int_0^\infty g(t) dt + \sum_{n=1}^\infty \frac{(-m_z)!}{n!(n-m_z)!} |\Phi_{m_z,n}\rangle\langle\Phi_{m_z,n}| \int_0^\infty t^n g(t) dt \\
&= |\Phi_{m_z,0}\rangle\langle\Phi_{m_z,0}| + \sum_{n=1}^\infty |\Phi_{m_z,n}\rangle\langle\Phi_{m_z,n}| = \mathbf{1}_{m_z},
\end{aligned} \tag{E.15}$$

where $t = |\tilde{\tau}|^2$ and $g(t)$ must satisfy

$$\int_0^\infty t^n g(t) dt = \begin{cases} 1 & \text{for } n = 0, \\ \frac{\Gamma(n+1)\Gamma(n-m_z+1)}{\Gamma(-m_z+1)} & \text{otherwise.} \end{cases} \tag{E.16}$$

Finally, putting together the sums over the m_z index of Eqs. (E.9) and (E.14), and recalling that $m_z = n - m$, we recover the completeness relation (E.4).

References

- [1] K. S. Novoselov, A. K. Geim, S. V. Morozov, D. Jiang, Y. Zhang, S. V. Dubonos, I. V. Grigorieva, and A. A. Firsov, “Electric field effect in atomically thin carbon films,” *Science*, vol. 306, no. 5696, p. 666, 2004.
- [2] Y. Zhang, Y.-W. Tan, L. S. Horst, and P. Kim, “Experimental observation of the quantum Hall effect and Berry’s phase in graphene,” *Nature*, vol. 438, no. 7065, p. 201, 2005.
- [3] A. H. Castro Neto, F. Guinea, N. M. R. Peres, K. S. Novoselov, and A. K. Geim, “The electronic properties of graphene,” *Rev. Mod. Phys.*, vol. 81, p. 109, Jan 2009.
- [4] M. Z. Hasan and C. L. Kane, “Colloquium: Topological insulators,” *Rev. Mod. Phys.*, vol. 82, pp. 3045–3067, Nov 2010.
- [5] X.-L. Qi and S.-C. Zhang, “Topological insulators and superconductors,” *Rev. Mod. Phys.*, vol. 83, pp. 1057–1110, Oct 2011.
- [6] S. Katayama, A. Kobayashi, and Y. Suzumura, “Electronic properties close to Dirac cone in two-dimensional organic conductor α -(BEDT-TTF) $_2$ I $_3$,” *The European Physical Journal B*, vol. 67, pp. 139–148, Jan 2009.
- [7] K. Kajita, Y. Nishio, N. Tajima, Y. Suzumura, and A. Kobayashi, “Molecular Dirac Fermion Systems – Theoretical and Experimental Approaches,” *Journal of the Physical Society of Japan*, vol. 83, no. 7, p. 072002, 2014.
- [8] V. M. Pereira, A. H. Castro Neto, and N. M. R. Peres, “Tight-binding approach to uniaxial strain in graphene,” *Phys. Rev. B*, vol. 80, p. 045401, 2009.

- [9] G. G. Naumis, S. Barraza-Lopez, M. Oliva-Leyva, and H. Terrones, “Electronic and optical properties of strained graphene and other strained 2D materials: a review,” *Reports on Progress in Physics*, vol. 80, p. 096501, aug 2017.
- [10] G. Tsoukleri, J. Parthenios, K. Papagelis, R. Jalil, A. C. Ferrari, A. K. Geim, K. S. Novoselov, and C. Galiotis, “Subjecting a graphene monolayer to tension and compression,” *Small*, vol. 5, no. 21, p. 2397, 2009.
- [11] M. Oliva-Leyva and G. G. Naumis, “Understanding electron behavior in strained graphene as a reciprocal space distortion,” *Phys. Rev. B*, vol. 88, p. 085430, 2013.
- [12] Y. Betancur-Ocampo, M. E. Cifuentes-Quintal, G. Cordourier-Maruri, and R. de Coss, “Landau levels in uniaxially strained graphene: A geometrical approach,” *Annals of Physics*, vol. 359, p. 243, 2015.
- [13] M. Oliva-Leyva and C. Wang, “Low-energy theory for strained graphene: an approach up to second-order in the strain tensor,” *Journal of Physics: Condensed Matter*, vol. 29, p. 165301, mar 2017.
- [14] M. Oliva-Leyva and C. Wang, “Magneto-optical conductivity of anisotropic two-dimensional DiracWeyl materials,” *Annals of Physics*, vol. 384, pp. 61 – 70, 2017.
- [15] E. Díaz-Bautista and D. J. Fernández, “Graphene coherent states,” *The European Physical Journal Plus*, vol. 132, p. 499, Nov 2017.
- [16] E. Díaz-Bautista, Y. Concha-Sánchez, and A. Raya, “Barut-Girardello coherent states for anisotropic 2D-Dirac materials,” *arXiv:1902.01995*, 2019.
- [17] J. Klauder and B. Skagerstam, *Coherent States*. World Scientific, 1985.
- [18] A. Feldman and A. H. Kahn, “Landau diamagnetism from the coherent states of an electron in a uniform magnetic field,” *Phys. Rev. B*, vol. 1, p. 4584, Jun 1970.
- [19] F. T. Arecchi, E. Courtens, R. Gilmore, and H. Thomas, “Atomic coherent states in quantum optics,” *Phys. Rev. A*, vol. 6, pp. 2211–2237, Dec 1972.
- [20] Y. K. Wang and F. T. Hioe, “Phase transition in the dicke model of superradiance,” *Phys. Rev. A*, vol. 7, pp. 831–836, Mar 1973.
- [21] W.-M. Zhang, D. H. Feng, and R. Gilmore, “Coherent states: Theory and some applications,” *Rev. Mod. Phys.*, vol. 62, pp. 867–927, Oct 1990.
- [22] S. T. Ali, J. P. Antoine, and J. P. Gazeau, *Coherent States, Wavelets, and Their Generalizations*. Springer, New York, NY, 2014.
- [23] V. Fock, “Bemerkung zur quantelung des harmonischen oszillators im magnetfeld,” *Zeitschrift für Physik*, vol. 47, p. 446, May 1928.

- [24] L. Page, “Deflection of electrons by a magnetic field on the wave mechanics,” *Phys. Rev.*, vol. 36, p. 444, Aug 1930.
- [25] C. G. Darwin, “The diamagnetism of the free electron,” *Mathematical Proceedings of the Cambridge Philosophical Society*, vol. 27, no. 1, p. 86, 1931.
- [26] I. A. Malkin and V. I. Man’ko, “Coherent states of a charged particle in a magnetic field,” *Soviet Physics JETP*, vol. 28, no. 3, p. 527, 1969.
- [27] R. J. Glauber, “Coherent and incoherent states of the radiation field,” *Phys. Rev.*, vol. 131, p. 2766, Sep 1963.
- [28] L. Landau, “Diamagnetismus der metalle,” *Zeitschrift für Physik*, vol. 64, p. 629, Sep 1930.
- [29] M. Rasetti, “Coherent states and partition function,” *International Journal of Theoretical Physics*, vol. 14, pp. 1–21, Sep 1975.
- [30] G. G. Cabrera, *A Coherent-State Representation of the Ground State of Quantum Antiferromagnets*, pp. 405–412. Boston, MA: Springer US, 1994.
- [31] A. Feldman and A. H. Kahn, “Landau diamagnetism from the coherent states of an electron in a uniform magnetic field,” *Phys. Rev. B*, vol. 1, pp. 4584–4589, Jun 1970.
- [32] J. P. Gazeau and P.-Y. Hsiao, *Orbital Magnetism of Two Dimensional Fock-Darwin Confined Electron Gas*, pp. 186–195. World Scientific Publishing, 2001.
- [33] J. P. Gazeau, P. Y. Hsiao, and A. Jellal, “Exact trace formulas for two-dimensional electron magnetism,” *Phys. Rev. B*, vol. 65, p. 094427, Feb 2002.
- [34] E. Díaz-Bautista, J. Negro, and L. M. Nieto, “Partial coherent states in graphene,” *Journal of Physics: Conference Series*, vol. 1194, p. 012025, 2019.
- [35] E. Drigho-Filho, Ş. Kuru, J. Negro, and L. M. Nieto, “Superintegrability of the Fock-Darwin system,” *Annals of Physics*, vol. 383, p. 101, 2017.
- [36] V. V. Dodonov, *Coherent states and their generalizations for a charged particle in a magnetic field*, pp. 311–338. Cham: Springer International Publishing, 2018.
- [37] M. M Novaes and J. P. Gazeau, “Multidimensional generalized coherent states,” *Journal of Physics A: Mathematical and General*, vol. 36, p. 199, dec 2002.
- [38] A. Dehghani, H. Fakhri, and B. Mojaveri, “The minimum-uncertainty coherent states for Landau levels,” *Journal of Mathematical Physics*, vol. 53, no. 12, p. 123527, 2012.
- [39] A. Dehghani and B. Mojaveri, “Generalized $su(2)$ coherent states for the Landau levels and their nonclassical properties,” *The European Physical Journal D*, vol. 67, no. 12, p. 264, 2013.

- [40] D. J. Fernández, J. Negro, and M. A. del Olmo, “Group approach to the factorization of the radial oscillator equation,” *Annals of Physics*, vol. 252, no. 2, p. 386, 1996.
- [41] K. Kikoin, M. Kiselev, and Y. Avishai, *Dynamical Symmetries for Nanostructures: Implicit Symmetries in Single-Electron Transport Through Real and Artificial Molecules*. Springer-Verlag Wien, 2012.